Effect of Air-Gap Distance on the Morphology and Thermal Properties of Polyethersulfone Hollow Fibers

TAI-SHUNG CHUNG,[1,2] XUDONG HU[1]

[1] Department of Chemical Engineering, National University of Singapore, 10 Kent Ridge Crescent, Singapore 119260

[2] Institute of Materials Research and Engineering, 10 Kent Ridge Crescent, Singapore 119260

Received 31 October 1996; accepted 26 April 1997

ABSTRACT: By using 30/70 polyethersulfone/NMP (*N*-methyl-2-pyrrolidone) solutions as an example, we have determined the role of air-gap distance on nascent fiber morphology, performance, and thermal properties. An increase in air-gap distance results in a hollow fiber with a less layer of fingerlike voids and a significant lower permeance. For the first time we have reported that the T_g of a dry-jet wet-spun fiber prepared from one-polymer/one-solvent systems is lower than that of a wet-spun fiber, and T_g decreases with an increase in air-gap distance. These interesting phenomena arise from the fact that different precipitation paths take place during the wet-spinning and dry-jet wet-spinning processes. Wet-spun fibers experience vigorous and almost instantaneous coagulations; it results in hollow fiber skins with a long-range random, unoriented chain entanglement, but loose structure. Dry-jet wet-spun fibers first go through a moisture-induced phase separation process and then a wet-phase inversion process; it results in external fiber skins with a short-range random, compact, and slightly oriented or stretched structure. As a result, the outskin of wet-spun fibers have a greater free volume and a higher first T_g than that of the dry-jet wet-spun ones. Both SEM (scanning electronic microscope) photomicrographs and DSC (differential scanning calorimeter) analyses support our conclusion. © 1997 John Wiley & Sons, Inc. J Appl Polym Sci **66:** 1067–1077, 1997

Key words: air-gap effect; asymmetric membrane; membrane formation; free volume; phase inversion

INTRODUCTION

The development of integrally skinned asymmetric membranes for gas and liquid separations has received a lot of attention. These membranes consist of a thin skin layer supported by a porous substructure. The skin layer determines the permeability and selectivity of the membrane, whereas the porous substructure functions primarily as a physical support for the skin. Both layers are composed of the same material and integrally bonded. Usually the skin layer has a thickness on the order of several hundred to several thousand angstroms. At present, hollow-fiber membranes successfully utilized for gas and liquid separations are mostly prepared from amorphous polymers by means of a phase inversion technique. In this technique, a polymer is dissolved in a suitable solvent or solvent mixtures and spun into a coagulation bath. Upon contact with the coagulation media, solvent exchange occurs between the extruded fiber and coagulant and yields the nascent membrane structure.

There are plenty of studies and reviews on

Corrrespondence to: T.-S. Chung (chencts@leonis.nus.sg).
Contract grant sponsor: National University of Singapore (NUS); contract grant number: 960609A.

Journal of Applied Polymer Science, Vol. 66, 1067–1077 (1997)
 CCC 0021-8995/97/061067-11

asymmetric polymer membranes. In short, they can be classified into four categories. A significant number of researches have been conducted in the area of understanding the inherent separation properties of a material as well as searching for high-performance membrane materials. The inventions of 6FDA–polyimides and tetrabromo–bisphenol A polycarbonates for gas-separation membrane applications are some examples.[1–5] Technology development on the fabrication of asymmetric membranes with an ultrathin dense layer has received remarkable attention from both academia and industry. This is due to the fact that the thinner the dense layer is, the higher the productivity is. Permea' graded-density skin asymmetric hollow fibers,[6] Koros and Pinnau's [University of Texas (UT)] extrathin asymmetric flat membranes,[7] and Hoechst Celanese' integrally skinned asymmetric and multilayer composite membranes[8,9] are examples of many latest inventions in membrane technology.

A large number of publications can be found in the area of membrane formation fundamentals. Although modern asymmetric membrane fabrication technologies are extensions of the Loeb-Sourirajan technique[10] developed for reverse osmosis (RO) applications about 30 years ago, there is a lack of knowledge in the detailed mechanisms of membrane formation. This is due to the fact that the fabrication of a hollow fiber with a desirable pore-size distribution and performance is not a trivial process. Many (possibly uncontrolable) factors control fiber morphology during the phase inversion, and a membrane develops its preliminary structure almost instantaneously in the precipitation stage. Many review articles have summarized the progress on the scientific understanding of asymmetric membranes; however, most of them are on flat asymmetric membranes.[11–16] Little attention has been given to hollow-fiber formation.

Many researchers have attempted to mathematically simulate flat membrane formation and investigate solvent exchange mechanisms using a variety of diffusion and solution theories.[17–20] However, there are a few unsolved questions. For instance, it is always a debatable issue if one can accurately calculate the phase diagram and quantitatively predict the phase inversion process during flat membrane formation. Hollow-fiber formation further complicates mathematical simulations. Fundamental understanding of hollow-fiber fabrication is still in the embryo stage. Recently, Chung and his coworkers[21,22] investigated the effect of air-gap distance and elongational stress on hollow-fiber formation.

The controlling factors for hollow fiber spinning are not only complicated, but also quite different from that for flat membranes. For example, there are two coagulations taking place in hollow-fiber spinning (internal and external surfaces), while there is only one major coagulation surface for an asymmetric flat-sheet membrane. If liquids are used as bore fluids, the internal coagulation process for a hollow fiber starts immediately after extrusion from a spinneret and then the fiber goes through the external coagulation, while there is usually a waiting period for an asymmetric flat membrane before immersing it into a coagulant. In addition, the spinning dope suitable for fabricating hollow fibers generally has a much greater viscosity and elasticity than that for flat membranes. Furthermore, the phase inversion process for hollow-fiber formation usually takes place nonisothermally under tension or elongational stress, while flat membranes do not experience this type of stress during the fabrication.

In this article, we attempt to continue our previous work to explore the relationship between spinning conditions and hollow-fiber formation. Our focus is to understand the effect of air-gap distance on asymmetric hollow-fiber performance and to characterize as-spun fiber morphology using thermal and SEM techniques.

EXPERIMENTAL

Materials

Polyethersulfone was generously provided by Prof. W. K. Teo at NUS (National U. of Singapore), purchased from Amoco Performance Products Inc., Ohio. It has a weight-average molecular weight of about 15,000. *N*-Methyl-2-pyrrolidone (NMP, 99+%), was supplied by Merck. Other organic solvents were reagent grade and used as received. This material has been studied by Teo's group at the NUS for gas-separation membranes[23] and by others.[11]

Spinning Device and Conditions

Figure 1 shows the schematic diagram of the hollow-fiber spinning apparatus. The spinning dope was extruded under a nitrogen pressure of 10 psi through a spinneret. The dimensions of this spinneret were 800 and 550 μm for outer diameter

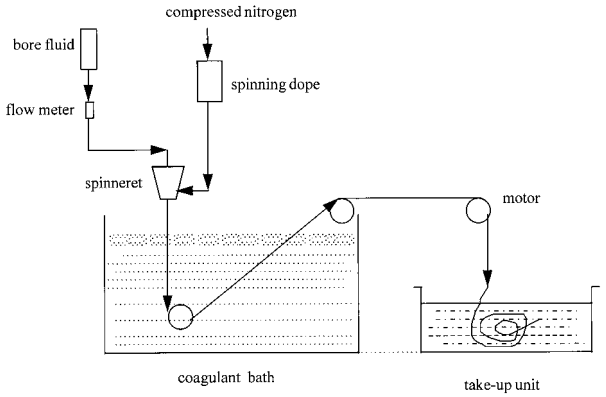

Figure 1 The schematic diagram of the hollow-fiber spinning process.

(o.d.) and inner diameter (i.d.), respectively. The bore fluid was conveyed by the gravity force and its flow rate was controlled by a flow meter. The spinning dope and the bore fluid met at the tip of the spinneret, then passed through an air gap ranging from 0–14.4 cm before entering the coagulation bath. Because the takeup speed was nearly the same as the fiber free-falling velocity in the coagulation bath, almost no external elongational stresses (except gravity) were applied to the nascent fibers. Once a hollow fiber was formed, it was stored in a water bath for 5 days and then transferred to a tank containing fresh methanol for 2 h to remove the residual NMP completely. Hollow fibers thus treated were used for further test and study. Table I summarizes the detailed process parameters and spinning conditions.

Scanning Electron Microscope (SEM)

Membrane samples for SEM study were first immersed in liquid nitrogen and fractured, and then sputtered with gold using a JEOL JFC-1100E Ion Sputtering Device. We employed both a JEOL™ JSM U3 electron microscope and a field emission scanning electron microscope Hitachi™ S-4100 to investigate fiber morphology.

Measurement of Glass Transitional Temperatures

The glass transitional temperatures (T_g) of as-spun and heat-treated hollow fibers were measured using a Netzsch(differential scanning calorimeter (DSC 200) with a heating rate of either 10 or 20°C/min from the room temperature to 300°C. Hollow fibers were cut into very small pieces and placed in DSC pans and weighed prior to sealing. All tests were repeated at least twice to ensure reproducibility. After the first DSC run (up to 300°C), the testing sample was cooled down to the ambient temperature and subsequently started with the second DSC run. Precision of the measurements was at least 1°C. The inflection temperature was chosen to define the glass transition temperature in these measurements.

Table I Process Parameters and Spinning Conditions

Process Parameters/Spinning Conditions	Value
1. Spinning solution	PES/NMP
2. Polymer concentration (by weight)	30%
3. Spinneret temperature (°C)	25
4. Viscosity at 25°C (cp)	8336
5. Spinneret OD/ID	0.8 mm/0.55 mm
6. Bore fluid composition	40/60 (NMP:H_2O)
7. Bore fluid flow rate (cc/min)	0.083
8. Dope pressure (psi)	10
9. Dope flow rate (cc/min)	0.317
10. Range of air-gap distance (cm)	0–14.4
11. Takeup velocity (cm/min)	72–115.2
12. Coagulant	H_2O
13. Coagulant temperature (°C)	25
14. Room relative humidity (%)	58
15. Drying procedure	1 day in water at 25°C 2 h in methanol at 25°C 1 day air dry at 25°C

Table II Permeance Change with Different Air-Gap Distance

Air Gap Distance (cm)	O_2 Flow Rate (GPU)	N_2 Flow Rate (GPU)	He Flow Rate (GPU)	Selectivity O_2/N_2
14.4	22.87	25.23	55.94	0.91
6.1	24.87	26.23	76.67	0.95
1.2	42.93	40.01	117.1	0.93
0	75.79	74.90	165.2	0.99

Module Fabrication and Tests

To characterize membrane performance as a function of air-gap distance, we use gas permeation cells. Two to five fibers with a length of 10 cm were assembled into bundles. One end of the bundles was sealed with a 5-min rapid solidified epoxy resin (Araldite™, Switzerland), while the shell side of the other end was glued onto an aluminum holder using a regular epoxy resin (Eposet™). It took 8 h to fully cure the Eposet™ resin. The prepared module was fitted into a stainless steel pressure cell for the gas permeation measurement.

The fluxes of gases through the hollow fiber module were determined using a bubble-flow meter and calculated by the following equation:

$$\text{Flux(permeance)} = \frac{Q}{\Delta PA} = \frac{Q}{n\pi Dt\Delta P}$$

where P is the permeability of the separation layer; t is the effective length of the fibers; ΔP is the transmembrane pressure drop; A is the membrane effective surface area; Q is the the gas permeation rate (cc/s) measured from a bubble meter; n is the number of tested fibers; D is the outer diameter of the fibers. We use GPU as the gas permeation units, and one GPU is equal to 1×10^{-6} cm^3 (STP) cm^{-2} s^{-1} $cmHg^{-1}$.

It is very important to point out that, similar to flat membranes, hollow fibers may also have pin holes in the skin. As a result, experimentists may obtain false results on permeance. These pin pores or defects can be easily detected by immersing modules underwater with a positive bore pressure of air. Only samples free of pin holes were employed in the data analysis.

RESULTS AND DISCUSSION

The Effects of Air-Gap Distance on Permeance and Fiber Morphology

Table II summarizes the flux change with the air-gap distance and clearly shows that air-gap distance plays a very important role on nascent fiber performance. An increase in air-gap distance results in a significant decrease in permeance. This interesting phenomenon may arise from the fact different precipitation paths take place during the

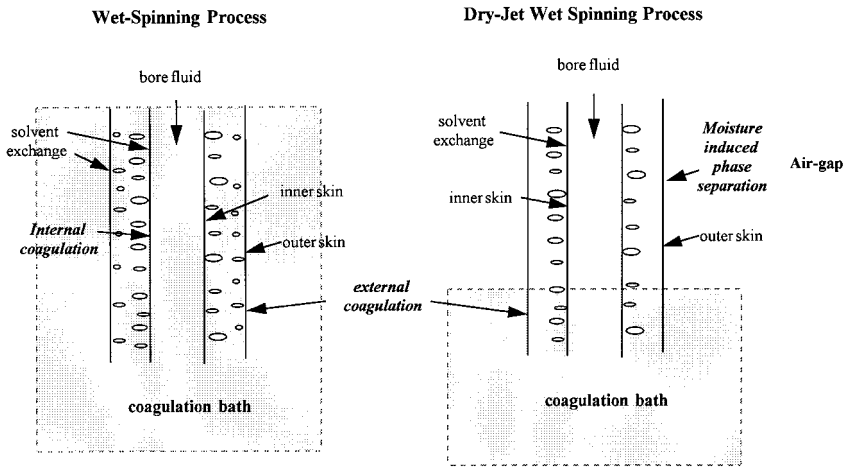

Figure 2 Precipitation in the wet-spinning and dry-jet wet-spinning process.

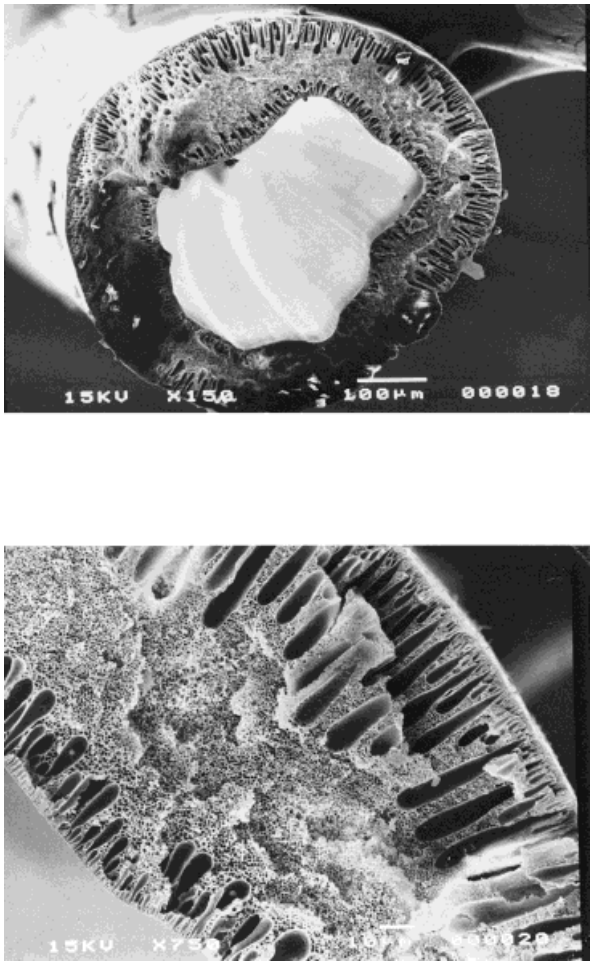

Figure 3 The cross-section morphology of hollow fibers spun with zero air-gap distance (wet-spun). (Top: ×150, bottom: ×750.)

wet-spinning and dry-jet wet-spinning process. As illustrated in Figure 2, the nascent hollow-fiber experiences "convective type" coagulations at its internal and external surfaces simultaneously in a wet-spinning process. However, the nascent fiber undergoes two coagulation paths in a dry-jet wet-spinning process. It first experiences a "convective-type" internal coagulation and a "nonconvective-type" external coagulation in the air-gas region, then rapid solvent exchange takes place in its external surface when the fiber is immersed in the coagulation bath. The "convective" term used here is to describe the vigorousness of the coagulation process because several reports have suggested that it, as well as observed convective flows, occurred during the precipitation of flat and hollow-fiber membranes.[8,9,22,25–27] Figures 3 and 4 show the cross-section morphology of hollow fibers spun with zero and 14.4 cm air-gap distances. Clearly, one can see the effect of air-gap distance on the fiber cross-section morphology. Fibers spun with an air-gap distance of 14.4 cm mainly have one array of fingerlike voids closed to the inner surface, while fibers spun with no air gap have two arrays of fingerlike voids closed to the inner and outer surface.

As pointed out by the previous authors,[22,25–27] fingerlike voids are probably created by spinodal decomposition with the aid of unbalanced localized stresses from surface tension, solvent/coagulant agglomeration, volumetric change, and radially convective flows of the inner and outer coagulants. The driving forces to produce fingerlike voids can be minimized if the spinning dope has a higher viscosity[8,9,22,27] and the fiber formation temperature is high.[22] Using Kesting et al.[11] and Chung et al.'s[22] results as examples, the former demonstrated that a multilayer fingerlike void structure could be easily formed in polysulfone

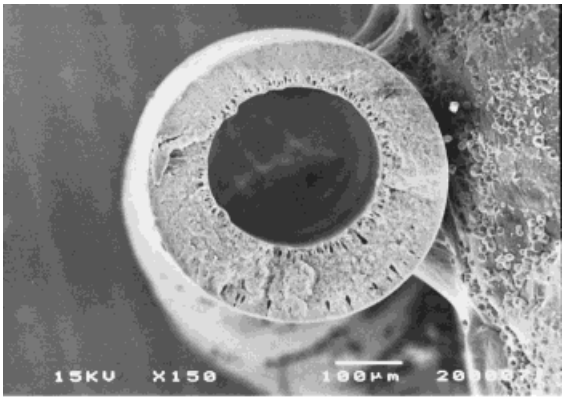

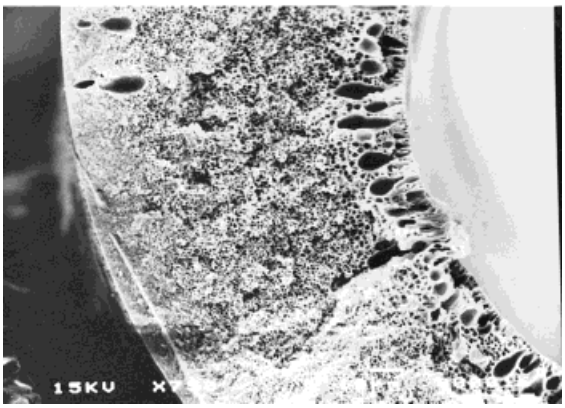

Figure 4 The cross-section morphology of hollow fibers spun with an air-gap distance of 14.4 cm. (Top: ×150, bottom: ×750.)

Table III Dimensional Change of Hollow Fibers as a Function of Air-Gap Distance

Air-Gap Distance (cm)	OD (cm)	ID (cm)	OD/ID Ratio	Cross-Section Area Change Ratio[a]
14.4	0.47	0.23	2.04	2.01
6.1	0.50	0.25	2.00	1.80
1.2	0.61	0.37	1.65	1.44
0	0.63	0.38	1.66	1.34

[a] Ratio of a fiber cross-section area to a spinneret cross-section area for fiber spinning.

hollow-fiber membranes if the dope contained 17 wt % of solids, while no fingerlike voids were observed in the cross section of hollow fibers spun from a concentration of 37 wt %. The latter exhibits that the fingerlike void structure in 6FDA–polyimide fibers can be completely eliminated when the fibers are spun at elevated coagulation temperatures.

In this study, the 30 wt % polyethersulfone dope has a relatively low viscosity. As a result, the wet-spun nascent fiber (Fig. 3) could not balance localized stresses created from rapid solvent exchange. This causes vigorous and convective-type coagulation and occurs at both the inner and outer surfaces. A double fingerlike void structure is therefore created in the cross section of wet-spun fibers. In the case of Figure 4, the external surface of the dry-jet wet-spun fiber contacted with the air first and went through a humid-induced phase-separation process. The condensed moisture permeates across the homogeneous surface mainly through a counterdiffusion (nonconvective) process. Compared to the rapid precipitation process that occurred in a wet-spun fiber, the humid-induced phase-separation process seems to be a much slower process. However, it has a significant and irreversible effect on final fiber morphology and performance. This is due to the fact that there are two mechanisms taking place in the air-gap region; namely, orientation and phase separation. Using Table III as an example, one can see that both the inner and outer diameters of dry-jet wet-spun fibers decrease with an increase in air-gap distance. Clearly, these decreases in i.d. and o.d. dimensions are due to the fact that air gap introduces an elongational stress on fibers because of gravity. The stress may have positive or negative effects on membrane formation and performance. A high elongational stress may pull molecular chains or phase-separated domains apart in the early stage of phase separation and create porosity, while a medium stress may induce molecular orientation and reduce membrane porosity or free volume. These two opposite phenomena have been

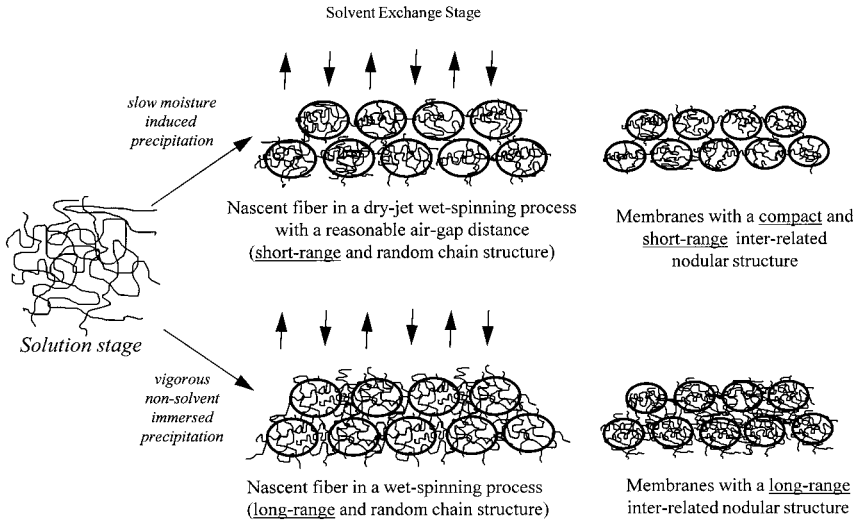

Figure 5 Skin morphology in the wet-spinning and dry-jet wet-spinning processes.

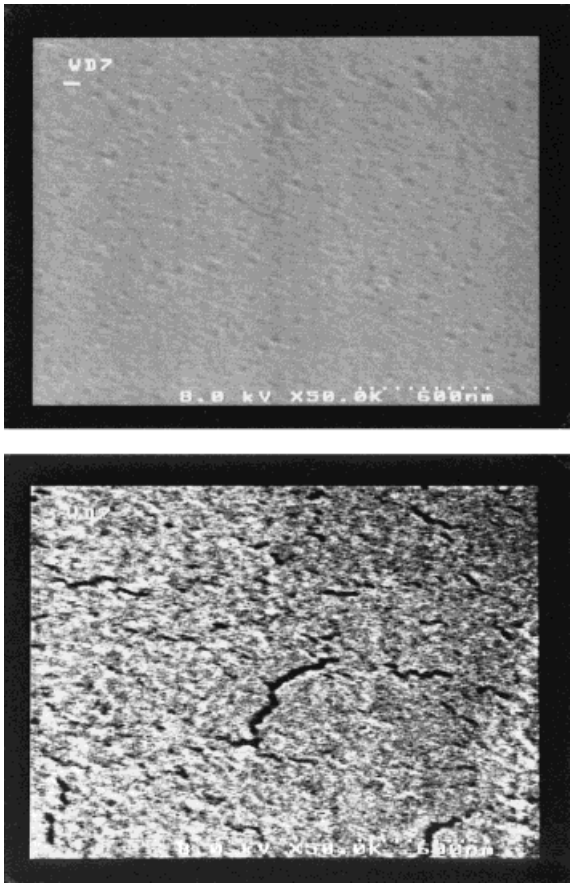

Figure 6 The surface morphology of hollow fibers spun with different air-gas distances. (Top: 0 cm, bottom: 14.4 cm, (magnification: ×50,000.)

discussed in details elsewhere for 6FDA–polyimide hollow-fiber membranes.[21,22] Because we observed permeance decreasing with an increase in air-gap distance, as shown in Table II, the most likely cause is that PES fibers spun from a big air-gap distance may have a greater orientation and tighter molecular packing than that of wet-spun fiber.

The relationship between permeance and air-gap distance can also be explained from the standpoint of chain conformation in a ternary solution. It is known that random flexible polymer chains tend to be fully swollen or extended in a good solvent. When adding a nonsolvent into a polymer solution, the extended random coil chains contract to reduce the Gibbs' free energy. The speed of chain contract depends on the rate of solvent exchange and the amount of the nonsolvent. In a wet-spinning process (Fig. 5) the as-spun fiber is immersed in the nonsolvent coagulation bath immediately after exiting from the spinneret. The coagulations at both inner and external surfaces are so vigorous and rapid that the extended random polymer chains contract suddenly and almost instantaneously. This results in a significant amount of nonsolvent and solvent trapped in the contracted chains. Both skin layers may, therefore, have a long-range random and unoriented polymeric chain interaction (entanglement) structure with some intermolecular voids (macro/microporosity or free volume). In the case of dry-jet wet-spinning process with a certain air-gap distance, the moisture-induced precipitation process slows the speed of chain contract and provides contracting chains with a time needed for conformation rearrangement. Therefore, the external surface layer prepared from a dry-jet wet-spinning process may have compact short-range random polymeric chain interactions (entanglement) in circumferential and lateral directions, and a slightly oriented and stretched structure in the axial direction. This type of skin morphology shall have a less macro and microporosity or free volume. Figure 6 shows the SEM pictures of external surface

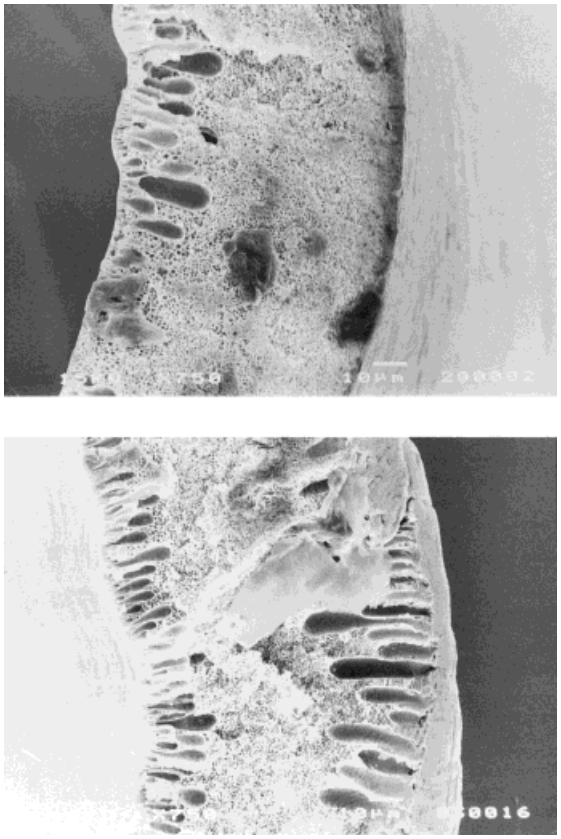

Figure 7 The cross-section morphology of hollow fibers spun with different air-gas distances. (Top: 6.1 cm, bottom: 1.2 cm, magnification: ×750.)

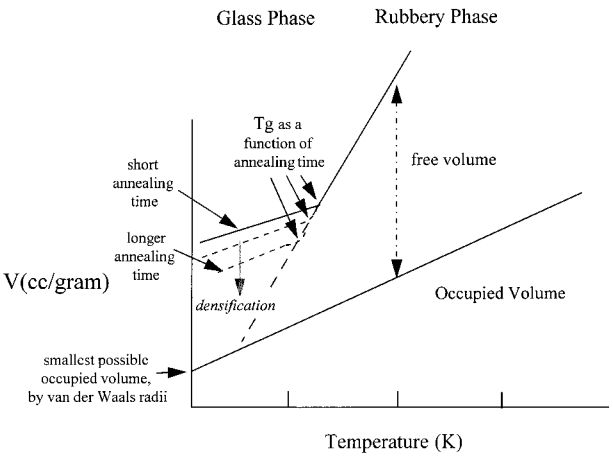

Figure 8 Qualitative illustration of the relationship among specific volume, T_g, and annealing time.[30,31]

of these fibers at 50,000 magnifications and their morphologies are consistent with our analysis. The wet-spun fibers do have a looser structure than dry-jet wet-spun fibers.

The O_2/N_2 selectivity data, shown in Table II, also confirm our hypothesis. The O_2/N_2 selectivity of 0.91–0.94 suggests that dry-jet wet-spun fibers have smaller pore sizes than that of wet-spun fibers. This is due to that fact that the gas selectivity in a Knudsen diffusion-controlled system is inversely proportional to the square root of their molecular weight ratio. In the case of O_2/N_2, the ideal selectivity is 0.935. Therefore, we are sure that the dry-jet wet-spun fibers separate O_2 and N_2 by means of Knudsen diffusion, while the wet-spun fibers have pore sizes almost too big to discern these two gases. In addition, the compact, slightly oriented and stretched outer skin structure in dry-jet wet-spun fibers tends to delay the liquid–liquid demixing process during the subsequent quench and immersion stage, one can easily see that fibers spun from an air-gap distance of 14.4 cm has a thicker and tighter cross-section morphology near the outer skin (Fig. 4) than the wet-spun ones (Fig. 3).

Figure 7 shows the cross-section morphology of fibers spun from air-gap distances of 6.1 and 1.2 cm. Their fiber cross-section structures are in agreement with our hypothesis. All fibers have a

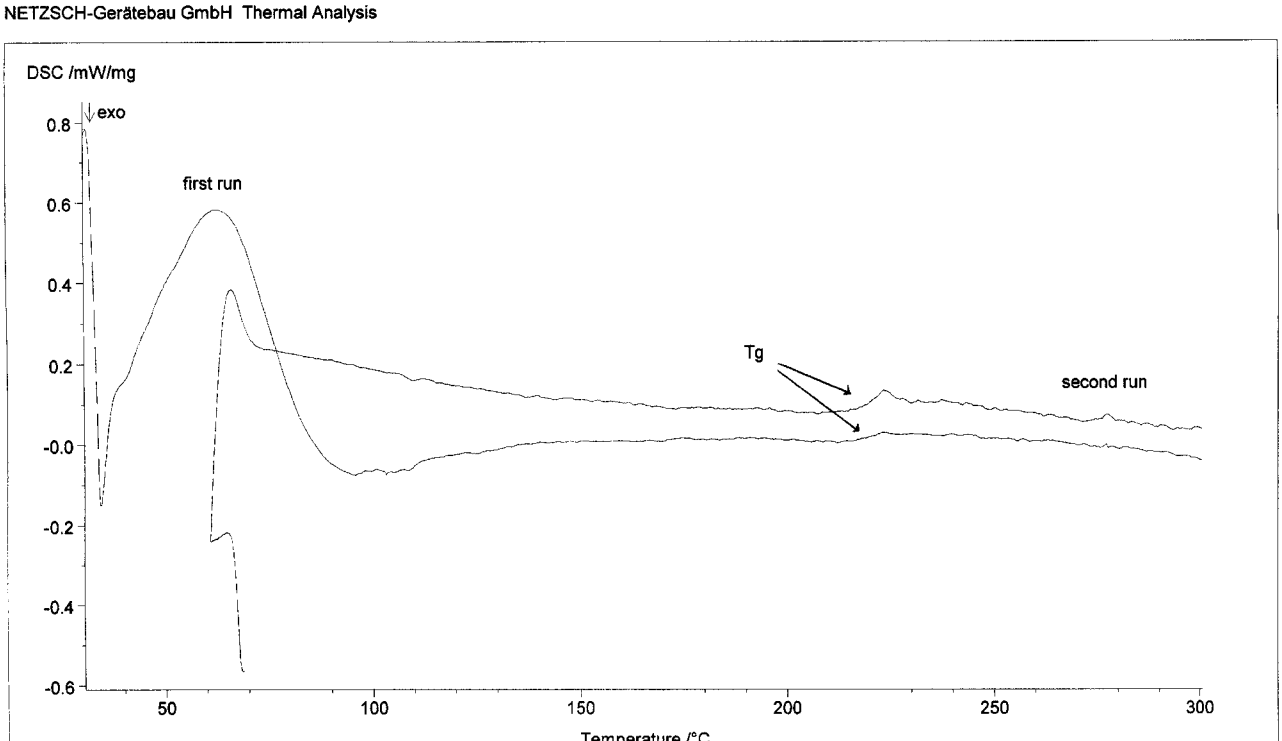

#	FILE	IDENTITY	SAMPLE	MASS/mg	DATE	SEGMENT	RANGE	CORR
1	JAND10	Jan-18-1996-D	PES hollow fiber	2.600	05.02.1996	1/ 4	30 °C/10.0/300 °C	000/Rg500 uV
2	JAND10	Jan-18-1996-D	PES hollow fiber	2.600	05.02.1996	3/ 4	30 °C/10.0/300 °C	000/Rg500 uV

Figure 9 Typical DSC curves of wet-spun hollow fibers with a heating rate of 10°C/min.

ring of fingerlike voids near the inner skin. The inner fingerlike void sizes increase with a decrease in air-gap distance. This may be due to the fact that the longer the air-gap distance, the less the laterally convective coagulation because of gravity. Fibers spun from an air-gap distance of 14.4 and 6.1 cm do not have a ring of fingerlike voids close to the outer skin due to the effect of moisture-induced phase-separation process and stress-induced orientation. If the air-gap distance is reduced to 1.2 cm, a layer of fingerlike voids close to the outer skin reappears because of the lack of moisture-induced phase-separation process and stress-induced orientation.

The Effects of Air-Gap Distance on T_gs of As-Spun Fibers

On a molecular scale, the glass transition temperature is the temperature above which the majority of bonds in polymeric chains have acquired sufficient thermal energy for rotational motion, or considerable torsional oscillation.[28] Below the T_g, the mobility of polymeric chains is so drastically reduced that the majority of polymeric chains have fixed conformations. T_g can also be defined as the temperature at which the thermal expansion coefficient changes in going from the rubbery to the glassy state.[29] It is a fact that when a slower cooling rate is employed to an amorphous polymeric melt in an otherwise identical experiment, the value of T_g observed varies considerably from that determined with a faster cooling rate.[30,31] Figure 8 qualitatively illustrates this phenomenon. The glass transition occurs at a lower temperature for a slower cooling rate, because a slower cooling rate allows more time for the molecules to approach their equilibrium state. A rapid quenched polymer possesses a higher free volume and exhibits a higher T_g than one quenched at a slower rate. To some degree, the phase inversion process occurred in the formation of a nascent hollow fiber is quite analogous to the rapid quench of a polymeric melt.[7,12] Any acceleration on fiber coagulation or melt quenching rate may result in similar effects on material morphology.

Figures 9 and 10 illustrate the typical DSC curves for wet-spun fibers. Figure 9 shows both the first run and the second run curves, and Figure 10 enlarges the first run curves shown in Figure 9. The first endothermic peak in Figure 9 indicates the evaporation of water. Because the DSC has been well calibrated, the based line variations in Figure 9 is in an acceptable range. The base line variations in Figure 10 are mainly due to the enlargement of the scale in y axis and the sensitivity of the DSC measurement. Similar variations have been observed in Permea's mem-

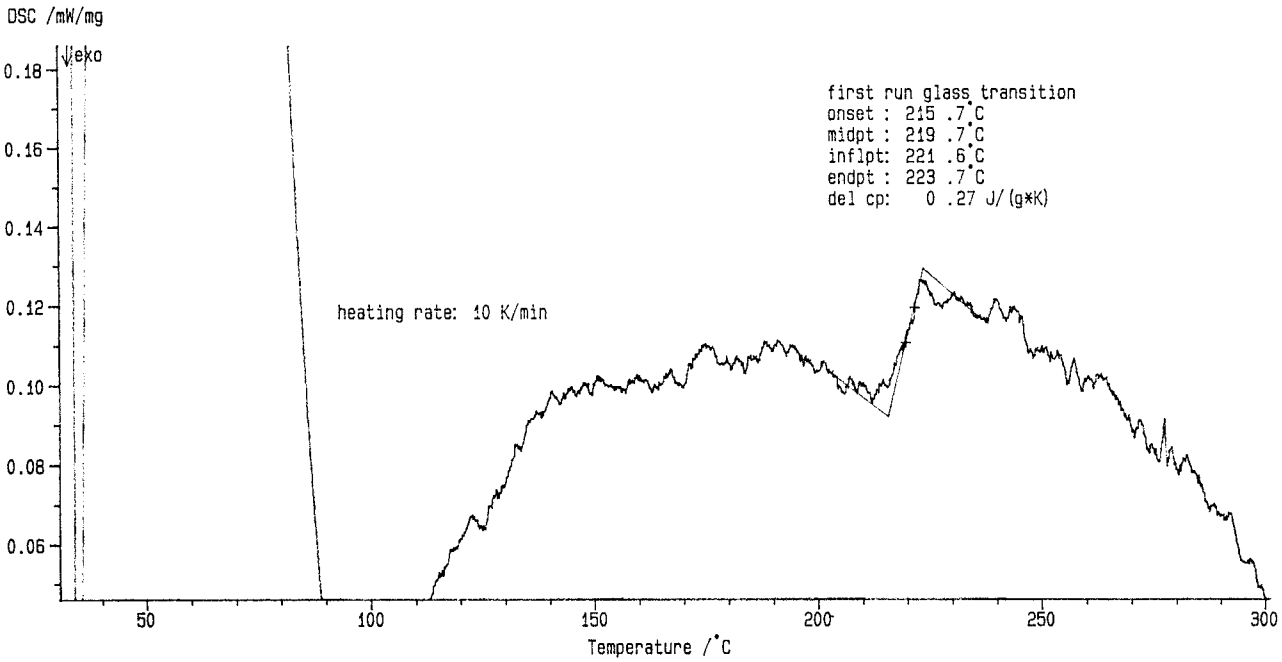

Figure 10 The enlarged first DSC curve of wet-spun hollow fibers with a heating rate of 10°C/min.

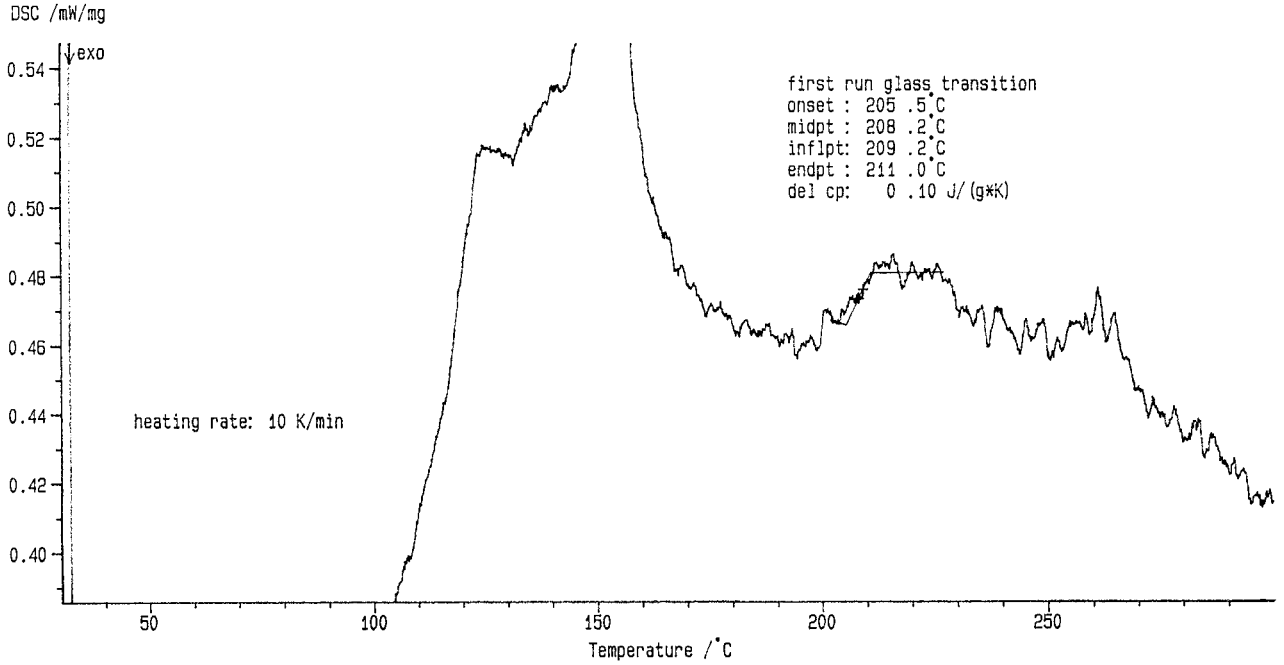

Figure 11 The enlarged first DSC curve of dry-jet wet-spun hollow fibers with an air-gap distance of 14.4 cm and a heating rate of 10°C/min.

branes.[6,11] Figure 11 illustrates the first DSC curve for dry-jet wet-spun fibers with an air gap distance of 14.4 cm. Table IV summarizes the T_g change as a function of air-gap distance for polyethersulfone membranes. The first-run T_g data suggest that an increase in air-gap distance results in a decrease in the T_g. After the first DSC run, samples lose memory of their previous history about the membrane formation; therefore, they have almost the same second-run T_g ($\sim$ 220–222°C). All DSC samples measured here have been immersed and rinsed in methanol for more than 2 h to remove any residual NMP in the testing samples. This is due to the known fact that residual NMP may affect the T_g.[32]

Because a wet-spun fiber has experienced vigorous and almost instantaneous coagulations, it tends to have both internal and external skins with a long-range random and unoriented chain entanglement but loose structure. A dry-jet wet-spun fiber experiences a much slower coagulation rate coupling with an elongational stress during the air-gap region, it has a short-range compact, and slightly oriented and stretched-chain structure. As a result, they have different responses during the DSC measurements. The slow compacted dry-jet wet-spun fibers have a structure closer to the equilibrium molecular packing state than the unoriented and quenched wet-spun fibers; therefore, the former have a T_g lower than that of the latter. This result is in agreement with the free-volume theory proposed by Kovacs[30] and Masuoka.[31]

Table IV Glass Transition Temperature of Polyethersulfone Hollow Fiber as a Function of Air-Gap Distance

Air-Gap Distance (cm)	First Run T_g (°C) (Heating Rate: 10 K/min)
0	221
1.2	221
6.1	216
14.4	209

CONCLUSION

By using polyethersulfone as an example, we have determined the role of air-gap distance on nascent fiber morphology, performance, and thermal properties. An increase in air-gap distance results in a hollow fiber with a less layer of fingerlike voids, a significant lower permeance, and a lower T_g. This interesting phenomenon may arise from the fact that different precipitation paths take place during the wet-spinning and dry-jet wet-spinning

processes. Wet-spun fibers tend to have a long-range random and unoriented chain entanglement with a loose external skin structure, while dry-jet wet-spun fibers tend to have a short-range compact, random, but oriented and stretched-tight structure. As a result, the outer skin of the former has a greater free volume and a higher first-run T_g than that of the latter. This result is in agreement with the free-volume theory proposed by Kovacs and Masuoka.

The authors thank Prof. W. K. Teo for the provision of us with PES materials and Ms. S. K. Teoh for her helpful comments and discussion. The authors thank the National University of Singapore (NUS) for its financial support of a research fund No. 960609A.

REFERENCES

1. W. J. Koros, G. K. Fleming, S. M. Jordan, T. H. Kim, and H. H. Hoehn, *Prog. Polym. Sci.,* **13,** 339 (1988).
2. S. A. Stern, Y. Mi, H. Yamamoto, and A. K. St. Clair, *J. Polym. Sci., Part B, Polym. Phys.,* **27,** 1887 (1989).
3. L. M. Robeson, *J. Membr. Sci.,* **62,** 165 (1991).
4. N. Muruganandam and D. R. Paul, *J. Membr. Sci.,* **34,** 185 (1987).
5. E. S. Sanders, Jr., J. A. Jensvold, D. O. Clark, F. L. Coan, H. N. Beck, W. E. Mickols, P. K. Kim, and W. Admassu, U.S. Pat. 4,955,993 (1990).
6. A. K. Fritzsche, M. K. Murphy, C. A. Cruse, R. F. Malon, and R. E. Kesting, *Gas Separat. Purificat.,* **3,** 106 (1989).
7. I. Pinnau and W. J. Koros, U.S. Pat. 4,902,422 (1990).
8. T. S. Chung, E. R. Kafchinski, and P. Foley, *J. Membr. Sci.,* **75,** 181 (1992).
9. T. S. Chung, E. R. Kafchinski, and R. Vora, *J. Membr. Sci.,* **88,** 21 (1994).
10. S. Loeb and S. Sourirajan, *Adv. Chem. Series,* **38,** 117 (1963).
11. R. E. Kesting and A. K. Fritzsche, *Polymeric Gas Separation Membranes,* John Wiley and Sons, New York, 1993.
12. I. M. Wienk, R. M. Boom, M. A. M. Beerlage, A. M. W. Bulte, C. A. Smolders, and H. Strathmann, *J. Membr. Sci.,* **113,** 361 (1996).
13. K. Kimmerle and H. Strathmann, *Desalination,* **79,** 283 (1990).
14. W. J. Koros and I. Pinnau, in *Polymeric Gas Separation Membranes,* D. R. Paul and Y. P. Yampol'skii, Eds., CRC Press, Boca Raton, FL, 1994, p. 209.
15. T. Matsuura, *Synthetic Membranes and Membrane Separation Process,* CRC Press, Boca Raton, FL, 1994.
16. J. Y. Lai, M. J. Liu, and K. R. Lee, *J. Membr. Sci.,* **86,** 103 (1994).
17. L. Yilmaz and A. J. McHugh, *J. Appl. Polym. Sci.,* **31,** 997 (1986).
18. C. Cohen, G. B. Tanny, and S. Prager, *J. Polym. Sci., Polym. Phys.,* **17,** 477 (1979).
19. P. Radovanovic, S. W. Thiel, and S. T. Hwang, *J. Membr. Sci.,* **65,** 231 (1992).
20. S. C. Pesek and W. J. Koros, *J. Membr. Sci.,* **88,** 1, (1994).
21. T. S. Chung, *J. Membr. Sci.,***126,** 19 (1997).
22. T. S. Chung, S. K. Teoh, and X. Hu, *J. Membr. Sci.,* to appear.
23. D. Wang, K. Li, and W. K. Teo, *J. Membr. Sci.,* **98,** 233 (1995).
24. H. Strathmann, K. Kock, P. Amar, and R. W. Baker, *Desalination,* **16,** 179 (1975).
25. I. Cabasso, *Synthesis Membranes, Vol. 1: Desalination,* A. F. Turbak, Eds., ACS Symp. Series 153, American Chemical Society, Washington, DC, 1981, p. 267.
26. L. Broens, F. W. Altena, C. A. Smolders, and D. M. Koenhen, *Desalination,* **32,** 33 (1980).
27. S. A. McKelvey and W. J. Koros, *J. Membr. Sci.,* **112,** 69 (1996).
28. J. Brandrup and E. H. Immergut, *Polymer Handbook,* VIII-61, John Wiley Sons, New York, 1966.
29. I. M. Ward, *Mechanical Properties of Solid Polymers,* Wiley-Interscience, New York, 1971.
30. J. J. Aklonis and A. J. Kovacs, in *Contemporary Topics in Polymer Science,* Vol. 3, M. Shen, Ed., Plenum Press, New York, 1979.
31. S. Matsuoka, *Polym. Eng. Sci.,* **21,** 908, (1981).
32. P. J. Brown, G. C. East, and J. E. McIntyre, *Polym. Commun.,* **31,** 156 (1990).